Enhancement of the visible light photocatalytic activity of heterojunction In$_2$O$_3$/BiVO$_4$ composites

**J. Z. Yin[1] · S. B. Huang[1,2] · Z. C. Jian[1] · M. L. Pan[1] · Y. Q. Zhang[1] ·
Z. B. Fei[1] · X. R. Xu[3]**

Abstract Novel In$_2$O$_3$/BiVO$_4$ heterojunction composite photocatalysts with tunable In$_2$O$_3$ content were prepared using a mild hydrothermal method. The structure, composition, and optical properties of the In$_2$O$_3$/BiVO$_4$ composites were determined by X-ray diffraction, scanning electron microscopy, transmission electron microscopy, UV–Vis diffuse reflectance spectroscopy, Brunauer–Emmett–Teller surface analysis, and X-ray photoelectron spectroscopy. Furthermore, photocatalytic activities of the as-prepared composites were investigated by studying the degradation of methylene blue (MB) solutions under simulated visible light irradiation ($\lambda > 420$ nm). It was found that the 50 % proportion of In$_2$O$_3$ in the In$_2$O$_3$/BiVO$_4$ composite exhibited the highest photocatalytic performance, leading to 91 % decomposition of MB within 240 min of irradiation.

1 Introduction

Nowadays, composite semiconductor materials with a heterojunction structure have been extensively exploited and applied in decomposition of organic pollutants and water splitting for hydrogen [1–6]. A heterojunction interface can be fabricated between the semiconductors with matching band potentials in composite semiconductor materials. As a consequence, a contact electric field is formed at this heterojunction interface. Driven by the contact electric field, photogenerated charges can transport from one semiconductor to another, leading to efficient separation of photogenerated electron–hole pairs [7, 8]. Therefore, looking for semiconductor materials with matching band potentials is very important for designing and constructing heterojunction semiconductors materials. Meanwhile, the study of the heterojunction effect on the behavior of photogenerated charges is also necessary and desired for the exploitation of composite materials with advanced functions.

As two of the most studied semiconductors, bismuth vanadate (BiVO$_4$) and indium oxide (In$_2$O$_3$) have been extensively investigated as gas sensors [9, 10] and photocatalysts [11–13]. With a narrow band gap of 2.4 eV [8], BiVO$_4$ displays a wide light response ability reaching the visible light region, but the electron–hole pairs have low separation efficiency. In$_2$O$_3$ is a semiconductor material, which possesses a direct band gap of 3.6 eV and an indirect band gap of 2.8 eV [14].

We all know that a heterojunction interface can be constructed between the semiconductors with matching band potentials in composite semiconductor materials. Accordingly, photogenerated charges can transport from one semiconductor to another. This favors the separation of photoinduced electrons and holes and thus enhances the photocatalytic activity of semiconductor heterostructure dramatically [15]. Considering the band gap of BiVO$_4$ ($E_g = 2.4$ eV) is lower than that of In$_2$O$_3$ ($E_g = 2.8$ eV), but the valence band (VB) of In$_2$O$_3$ ($E_{VB} = 2.17$ eV vs. NHE) is lower than that of BiVO$_4$ ($E_{VB} = 2.75$ eV vs. NHE). Therefore, it can be found that the energy levels of In$_2$O$_3$ and BiVO$_4$ are well matched, and an efficient heterostructure could be formed for the separation of photogenerated charge carriers when coupling them together.

✉ S. B. Huang
 chshuang@scut.edu.cn

1 School of Environment and Energy, South China University of Technology, Guangzhou 510006, China

2 State Key Laboratory of Pulp and Paper Engineering, South China University of Technology, Guangzhou 510640, China

3 Analytical and Testing Center, South China University of Technology, Guangzhou 510640, China

Motivated by the above concerns, in this work, we successfully fabricated various $In_2O_3/BiVO_4$ heterojunction photocatalysts using a hydrothermal method. To the best of our knowledge, the photocatalytic activity of $In_2O_3/BiVO_4$ composites has not been previously reported. The photocatalytic efficiency of the prepared photocatalysts was correlated with the $In_2O_3/BiVO_4$ mole ratio by studying the degradation of methyl blue (MB) under visible light irradiation. A possible mechanism of visible photocatalysis in $In_2O_3/BiVO_4$ heteroarchitectures was also proposed.

2 Experimental methods

2.1 Sample synthesis

All chemicals applied in experiment were analytical grade and used without further purification. The indium nitrate pentahydrate ($In(NO_3)_3 \cdot 5H_2O$) solutions were added to the solution of bismuth nitrate pentahydrate ($Bi(NO_3)_3 \cdot 5H_2O$) and ammonium vanadate (NH_4VO_3) (1:1 mol ratio) to form suspensions with different Bi/In mole ratios. The pH of the mixtures was then adjusted to 7 by slowly adding NaOH solution. After that, the suspension was transferred to a stainless autoclave where the hydrothermal reaction was carried out at 180 °C and maintained at that temperature for 24 h. Finally, the $In_2O_3/BiVO_4$ composites were collected by filtration and calcined at 500 °C for 2 h. The high-purity bismuth vanadate ($BiVO_4$) and pure In_2O_3 photocatalyst were also prepared by the same procedure. All of the composite samples were labeled as IxBy where I and B stand for In_2O_3 and $BiVO_4$, respectively, and x and y stand for the respective molar amounts in the composites (shown in Table 1).

2.2 Material characterization

Crystalline phases of the composites were subjected to X-ray diffraction (XRD) analysis (Bruker D8 Advance). The morphology, particle size, and microstructures of the

Table 1 Surface area and energy gaps of pure $BiVO_4$, pure In_2O_3 and various $In_2O_3/BiVO_4$ composites

Sample	In/Bi mole ratio	S_{BET} ($m^2\ g^{-1}$)	E_g (eV)
$BiVO_4$	–	0.19	2.31
I1B9	1:9	0.26	2.28
I3B7	3:7	1.68	2.29
I5B5	5:5	10.75	2.29
I7B3	7:3	18.28	2.08
I9B1	9:1	9.78	2.12
In_2O_3	–	1.86	2.59

samples were examined by scanning electron microscopy (SEM) (Model ZEISS, MERLIN Compact) and transmission electron microscopy (TEM) (JEOL, Model JEOL-2100). The UV–Vis diffuse reflectance spectra were recorded on a UV–Vis spectrophotometer (Shimadzu, Model UV-2450). A Brunauer–Emmett–Teller specific surface area instrument (American Micromeritics Instrument Corporation ASAP 2020 N) was used to measure the specific surface areas of the samples. X-ray photoelectron spectroscopy (XPS) measurements were taken on a British Kratos Axis Ultra DLD system with Al Kα radiation as the excitation source.

2.3 Photocatalytic activity studies

Photocatalytic activities of the samples were evaluated by decolorization of methylene blue (MB) aqueous solutions under simulated visible radiation. A 500-W halogen lamp (Foshan Fengjiang Modulator Tube Plant) equipped with a 420-nm cutoff glass filter was used as visible light source in this study. The concentration of MB solutions was 10 mg L^{-1}.

Typically, 0.05 g of a catalysts was added into 100 mL of MB solution. Prior to illumination, the solutions were stirred for 30 min in the dark, in order to reach the adsorption–desorption equilibrium. At a given time intervals, a 5-mL suspension was collected and filtered (MicroPES 0.45-μm membrane filter) to remove the photocatalyst particles. The concentration of MB was then determined by measuring the absorbance at $\lambda_{max} = 664$ nm, using a UV–Vis spectrophotometer (Shimadzu, Model UV-2450).

3 Results and discussion

3.1 XRD analysis of $In_2O_3/BiVO_4$ composites

XRD patterns of the $In_2O_3/BiVO_4$ composites compared with those of pure $BiVO_4$ and pure In_2O_3 are shown in Fig. 1. By comparing the standard card of the Joint Committee Power, the characteristic peaks appearing in the XRD patterns of pure $BiVO_4$ and pure In_2O_3 can be identified as peaks of monoclinic $BiVO_4$ (JCPDS No. 75-1866) and cubic In_2O_3 (JCPDS No. 06-0416), suggesting that in each sample both $BiVO_4$ and In_2O_3 solids have been formed with a good crystallinity. The diffraction peaks of monoclinic $BiVO_4$ are gradually intensified as the concentration of In_2O_3 increased from 10 to 50 %, and there was no obvious diffraction peak corresponding to In_2O_3. Upon further increasing the mole ratio of In_2O_3 in the composites, cubic In_2O_3 can be seen in the composites. Particularly, when the mole ratio of In_2O_3 was 90 %, the
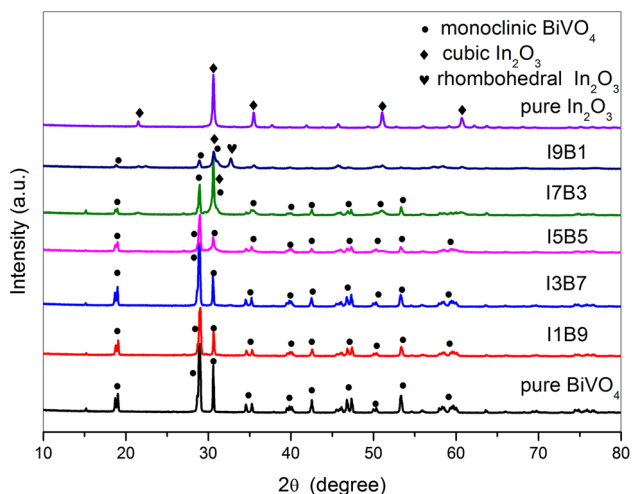
Fig. 1 XRD patterns of pure BiVO$_4$, pure In$_2$O$_3$, and In$_2$O$_3$/BiVO$_4$ composites with different mole ratios

cubic In$_2$O$_3$ was accompanied by diffraction peaks assigned to rhombohedral In$_2$O$_3$ (JCPDS No. 22-0336).

3.2 SEM and TEM analysis

The morphology and crystal structure of pure BiVO$_4$, pure In$_2$O$_3$, and an I5B5 sample were obtained from SEM and TEM images. The SEM image in Fig. 3a shows that the pure BiVO$_4$ was nubbly and applanate structure with an average width of 2–3 μm. The morphology of pure In$_2$O$_3$ (Fig. 2b) was cubic-shaped particles with a diameter in the range of 300–500 nm. Figure 2c, d shows the presence of In$_2$O$_3$ nanoparticles deposited on the BiVO$_4$ surface.

The TEM images of Fig. 2e, f show the morphology of pure BiVO$_4$ and pure In$_2$O$_3$, respectively. It can be seen that the shape of pure BiVO$_4$ was plate-like with a width of 1.5–2 μm and the shape of pure In$_2$O$_3$ was quadrate with a diameter about 100–300 nm, which agreed well the SEM image. As shown in Fig. 3f, g, two different crystal structures were observed on the composite surface, which can be assigned to BiVO$_4$ and In$_2$O$_3$, suggesting that the In$_2$O$_3$/BiVO$_4$ composites were successfully prepared with In$_2$O$_3$ nanoparticles covering the BiVO$_4$ surface.

3.3 UV–Vis diffuse reflectance spectroscopy

The UV–Vis diffuse reflectance spectra of BiVO$_4$, In$_2$O$_3$, and In$_2$O$_3$/BiVO$_4$ composites are shown in Fig. 3. It can be found that the absorption edges of the pure BiVO$_4$ and In$_2$O$_3$ occurred at about 535 and 478 nm, respectively. The band gap energies of BiVO$_4$ and In$_2$O$_3$ were estimated to be 2.31 and 2.59 eV, respectively, and were calculated using the equation [8]
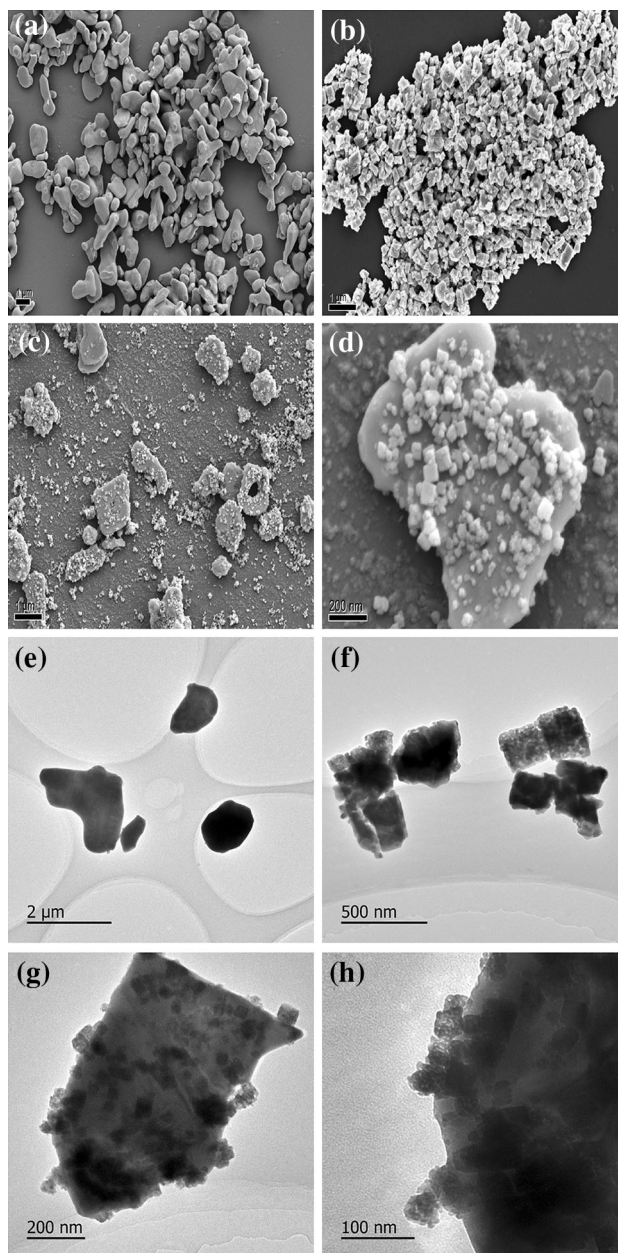

Fig. 2 SEM micrographs of **a** pure BiVO$_4$, **b** pure In$_2$O$_3$, and **c**, **d** I5B5 sample. TEM images of **e** pure BiVO$_4$, **f** pure In$_2$O$_3$, and **g**, **h** I5B5 sample

$$\lambda_g = 1239.8/E_g \qquad (1)$$

where λ_g and E_g represent constant band gap wavelength and band gap energy, respectively. The band gap energies of the In$_2$O$_3$/BiVO$_4$ composites given in Table 1 were calculated in the same way. Table 1 shows that all of In$_2$O$_3$/BiVO$_4$ composites possessed lower band gap energy than pure BiVO$_4$ (2.31 eV) and In$_2$O$_3$ (2.59 eV), indicating that the In$_2$O$_3$/BiVO$_4$ composites can lead to higher photocatalytic performance due to the production of more electron–hole pairs under visible light irradiation [4].
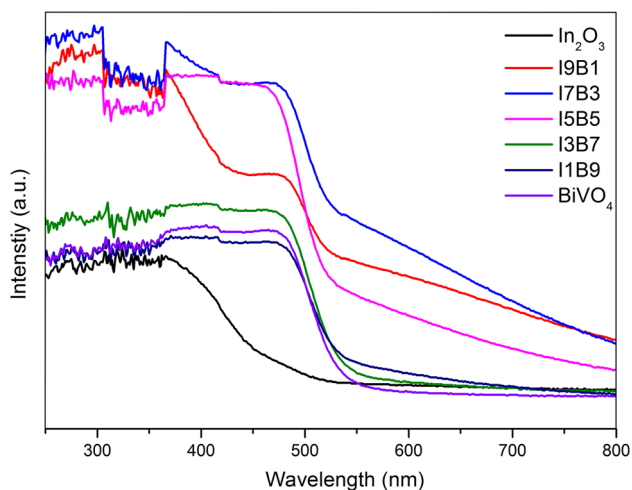
Fig. 3 UV–Vis diffuse reflectance spectra of pure BiVO$_4$, pure In$_2$O$_3$, and different mole ratios of In$_2$O$_3$/BiVO$_4$

3.4 BET analysis

Table 1 shows that the S$_{BET}$ of pure BiVO$_4$ and pure In$_2$O$_3$ were 0.19 and 1.86 m g^{-1}, respectively. It was worth noting that all of the composite catalysts exhibited a larger BET surface area than the pure BiVO$_4$. Furthermore, the composite catalysts showed a gradual increase in specific surface area when the mole ratio of In$_2$O$_3$ increased from 10 to 70 % and then decreased when it reached 90 %. Therefore, it could be concluded that the addition of In$_2$O$_3$ in BiVO$_4$ obtained larger specific surface area than pure BiVO$_4$.

3.5 XPS analysis

X-ray photoelectron spectroscopy (XPS) was employed to characterize the valance states and the surface chemical compositions. The I5B5 sample were investigated by XPS analysis, as shown in Fig. 4. According to the XPS observations (Fig. 4a), only C, Bi, O, V, and In elements were detected in the sample. The observed peak of C1s at 284.6 eV is attributed to the signal from carbon in the instrument [7, 16]. (The other XPS spectrum figures are presented in the Supporting Information.) In the Bi 4f region (Fig. 4b), the peaks at 158.9 and 164.2 eV are assigned to the Bi 4f$_{7/2}$ and Bi 4f$_{5/2}$, respectively, confirming that the bismuth species in In$_2$O$_3$/BiVO$_4$ is Bi^{3+} [17]. The peaks at about 523.9 and 516.7 eV (Fig. 4c) correspond to V 2p$_{1/2}$ and V 2p$_{3/2}$, respectively [18]. In the O 1s region (Fig. 5d), there are three types of oxygen energy levels existing in I5B5 composite. These can be attributed to lattice oxygen in metal oxides, such as In$_2$O$_3$ and BiVO$_4$ at 529.5 eV, hydroxyl groups at 531.4 eV, and chemisorbed water at 532.8 eV [17]. In Fig. 4e, two peaks for In 3d at 444.8 and 452.4 eV are assigned to In 3d$_{5/2}$ and

In 3d$_{3/2}$, respectively [15, 19]. Thus, it can be concluded that the In in the composite is likely in the 3+ oxidation state.

3.6 Photocatalytic activity for methylene blue (MB) degradation

Figure 5 shows the degradation efficiencies of MB solution over the pure BiVO4, pure In$_2$O$_3$, and In$_2$O$_3$/BiVO$_4$ composites. As shown in Fig. 5, the blank test in the absence of photocatalyst demonstrates that there is only a minor decrease in MB concentration under visible light irradiation, indicating that the photoinduced self-decomposition can be neglected. Fig. 5 shows that the degradation efficiency of MB within 240-min illumination was about for pure BiVO$_4$, pure In$_2$O$_3$, I1B9, I3B7, I5B5, I7B3, and I9B1, respectively. It is obvious that all of In$_2$O$_3$/BiVO$_4$ composites exhibited higher photocatalytic activity than that of pure BiVO$_4$ and In$_2$O$_3$. Furthermore, it also can be found that the photocatalytic activity of the coupled In$_2$O$_3$–BiVO$_4$ composites catalysts within 240 min of irradiation increases, reaches a maximum value, and then decreases as the proportion of In$_2$O$_3$ increases from 0 to 90 %, suggesting that there exists an optimal mole ratio for In$_2$O$_3$/BiVO$_4$ composites. Apparently, when the mole ratio of In$_2$O$_3$/BiVO$_4$ at 5:5 is found to have the highest photocatalytic activity, exhibiting the highest MB degradation of 91 % was obtained after 240 min of irradiation.

The results indicate that the In$_2$O$_3$/BiVO$_4$ composite highly reduces the electron–hole recombination rate and significantly enhances the photocatalytic performance. This enhancement in the photocatalytic performance for In$_2$O$_3$/BiVO$_4$ composites can be mainly attributed to the presence of the heterojunction structures at the interface of In$_2$O$_3$ and BiVO$_4$, where the photogenerated electron–hole pairs can have improved charge separation efficiency and increased charge carrier lifetime that result in enhanced photocatalytic activity [7, 8, 20]. Otherwise, the larger surface area and the stronger visible light response ability visible of In$_2$O$_3$/BiVO$_4$ composites comparing with pure BiVO$_4$ also had an important positive effect on the promotion of photocatalytic activity.

For the heterogeneous In$_2$O$_3$/BiVO$_4$ composites, the conduction band (CB) and valence band (VB) of semiconductors at the point of zero charge can be estimated using the following equation [4, 21, 22]

$$E_{VB} = X - E^e + 0.5E_g \tag{2}$$

$$E_{CB} = E_{VB} - E_g \tag{3}$$

where E_{VB} is the VB potential, X is the absolute electronegativity of the semiconductor (X is 6.035 [21] and
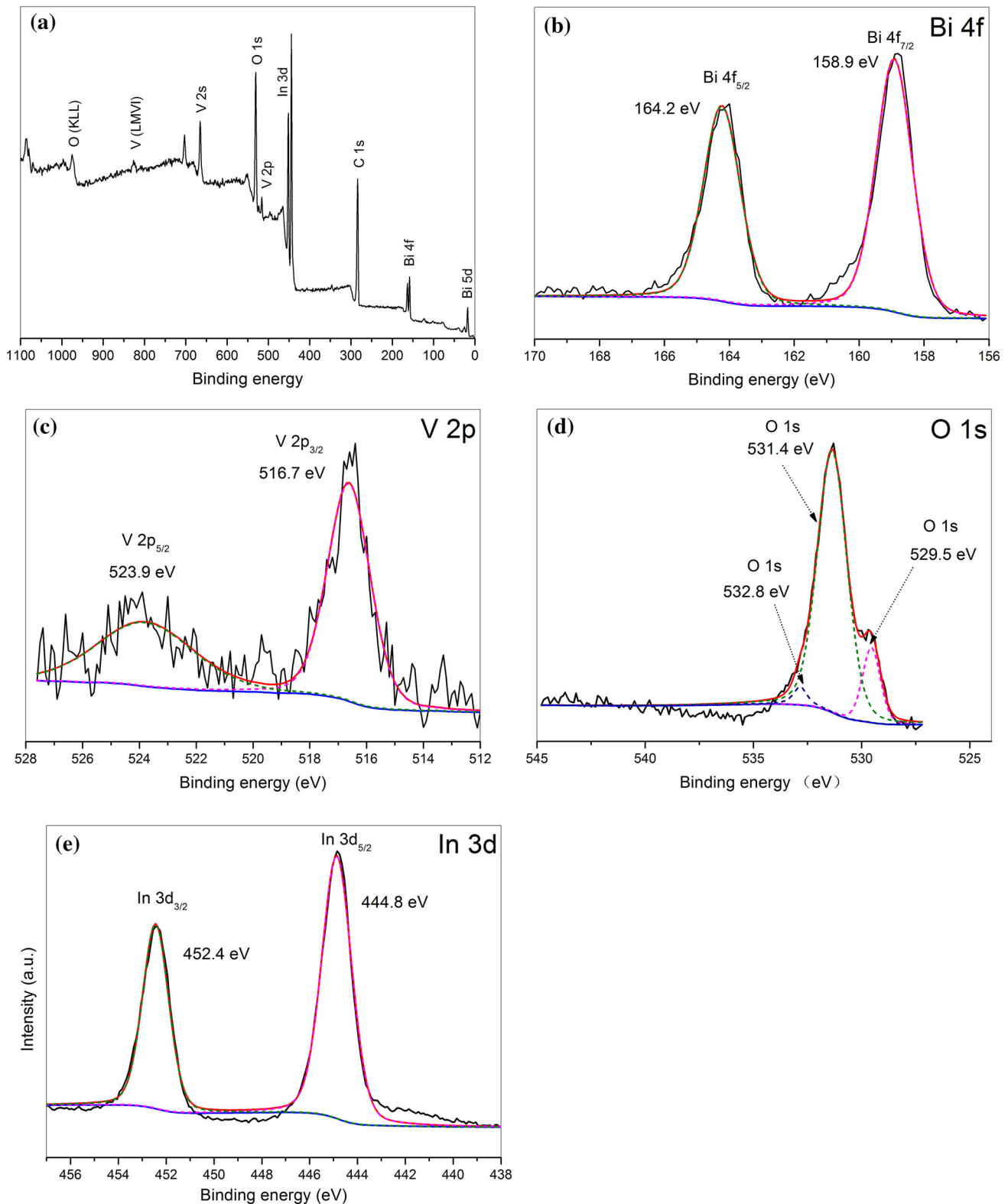
Fig. 4 XPS spectra of the I5B5: **a** typical XPS survey, **b** Bi 4f, **c** V 2p, **d** O1s, and **e** In 3d spectra

5.27 eV [15] for BiVO$_4$ and In$_2$O$_3$, respectively), E^e is the energy of free electrons on the hydrogen scale (4.5 eV), and E_g is the band gap energy of the semiconductor. The band gap values of In$_2$O$_3$ and BiVO$_4$ are 2.59 and 2.31 eV, respectively. From the above equation, the calculated results were E_{VB}
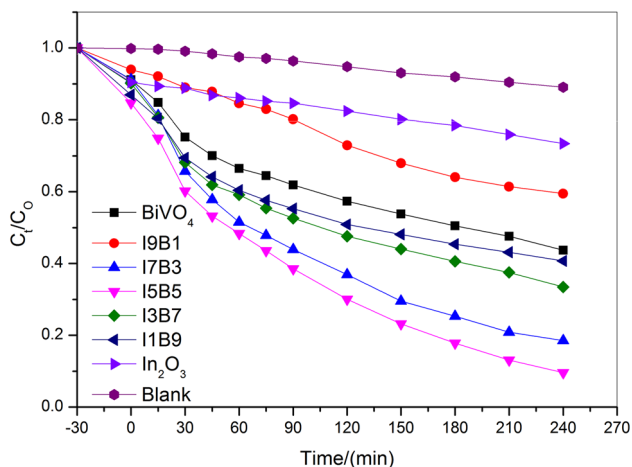
Fig. 5 Photodegradation efficiency of MB using pure BiVO$_4$, pure In$_2$O$_3$, and In$_2$O$_3$/BiVO$_4$ composites

(In$_2$O$_3$) = 2.06 eV, E_{CB} (In$_2$O$_3$) = −0.52 eV and E_{VB} (BiVO$_4$) = 2.69 eV, E_{CB} (BiVO$_4$) = 0.38 eV.

Figure 6 shows a schematic diagram of energy band structures of In$_2$O$_3$/BiVO$_4$, which is similar to that of the well-studied Co$_3$O$_4$/BiVO$_4$ [1] composites. Figure 6 shows that when BiVO$_4$ was irradiated by visible light ($\lambda > 420$ nm), the electrons in the VB of BiVO$_4$ were excited to its CB, leading to the generation of holes in its VB. The VB of In$_2$O$_3$ was more negative than that of BiVO$_4$, resulting in a local electric field [8, 21, 23]. As a consequence, the generation of holes in its VB tends to transfer from the VB of BiVO$_4$ to the VB of In$_2$O$_3$ at the interface, whereas the electrons remained in the CB of BiVO$_4$. Thus, the photoinduced charge carriers in BiVO$_4$ can be effectively separated and their recombination inhibited. As is known to all, the efficient charge separation can enhance and promote the photocatalytic activity of catalysts. Therefore, the In$_2$O$_3$/BiVO$_4$ composites with
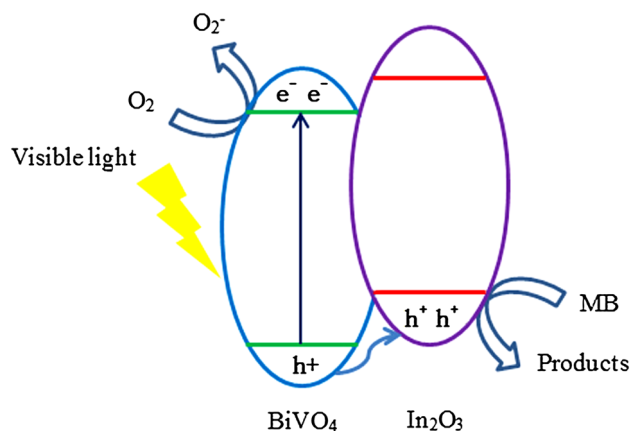
appropriate contents of In$_2$O$_3$ can demonstrate higher photocatalytic efficiencies than pure BiVO$_4$ particles.

4 Conclusions

In summary, a series of In$_2$O$_3$/BiVO$_4$ heterojunction photocatalysts were successfully fabricated via a mild hydrothermal method.

Through the photocatalytic tests using aqueous MB as a target contaminant under simulated visible light irradiation, it was found that the mole ratio of In$_2$O$_3$ to BiVO$_4$ in the In$_2$O$_3$/BiVO$_4$ composites had important effect on the degradation of MB under simulated visible light irradiation, and when the proportion of In$_2$O$_3$ in the In$_2$O$_3$/BiVO$_4$ was 50 %, it exhibited the highest photocatalytic activity for degradation of MB. The enhancement of photocatalytic performance of In$_2$O$_3$/BiVO$_4$ composites (I5B5), compared with that of pure BiVO$_4$, is mainly attributable to the formed heterogeneous structures at the interface of In$_2$O$_3$ and BiVO$_4$, and the lower band gap energy and the larger surface area of In$_2$O$_3$/BiVO$_4$ composites for pure BiVO$_4$ also can enhance its photocatalytic activity.

Fig. 6 Possible photocatalytic mechanism for degradation of MB over In$_2$O$_3$/BiVO$_4$ composite catalysts under simulated visible light irradiation

References

1. M.C. Long, W.M. Cai, J. Cai, B.X. Zhou, X.Y. Chai, Y.H. Wu, J. Phys. Chem. B **110**, 20211 (2006)
2. S.Q. Peng, Y.H. Huang, Y.X. Li, Mater. Sci. Semicond. Process. **16**, 62 (2013)
3. M.T. Niu, F. Huang, L.F. Cui, P. Huang, Y.L. Yu, Y.S. Wang, ACS Nano **4**, 681 (2010)
4. N. Wetchakun, S. Chaiwichain, B. Inceesungvorn, K. Pingmuang, S. Phanichphant, A.I. Minett et al., ACS Appl. Mater. Interfaces **4**, 3718 (2012)
5. L.L. Zhang, G.Q. Tan, S.S. Wei, H.J. Ren, A. Xia, Y.Y. Luo, Ceram. Int. **39**, 8597 (2013)
6. N. Wetchakun, S. Chainet, S. Phanichphant, K. Wetchakun, Ceram. Int. **41**, 5999 (2015)
7. J. Su, X.X. Zou, G.D. Li, X. Wei, C. Yan, Y.N. Wang et al., J. Phys. Chem. C **115**, 8064 (2011)
8. Z. He, Y. Shi, C. Gao, L. Wen, J. Chen, S. Song, J. Phys. Chem. C **118**, 389 (2013)
9. X. Chi, C.B. Liu, Y. Li, H.Y. Li, L. Liu, X.Q. Bo et al., Mater. Sci. Semicond. Process. **27**, 494 (2014)
10. P. Li, H.Q. Fan, Y. Cai, Colloids Surf. A **453**, 109 (2014)
11. Z.M. Li, P.Y. Zhang, J.G. Li, T. Shao, J. Wang, L. Jin, Catal. Commun. **43**, 42 (2014)
12. Y.C. Lu, C.C. Chen, C.S. Lu, J. Taiwan Inst. Chem. Eng. **45**, 1015 (2014)
13. J.J. Sun, X.Y. Li, Q.D. Zhao, J. Ke, D.K. Zhang, J. Phys. Chem. C **118**, 10113 (2014)

14. L.Y. Chen, W.D. Zhang, Appl. Surf. Sci. **301**, 428 (2014)
15. J.B. Mu, B. Chen, M.Y. Zhang, Z.C. Guo, P. Zhang, Z.Y. Zhang et al., ACS Appl. Mater. Interfaces. **4**, 424 (2011)
16. L. Chen, R. Huang, Y.J. Ma, S.L. Luo, C.T. Au, S.F. Yin, RSC Adv. **3**, 24354 (2013)
17. S. Chala, K. Wetchakun, S. Phanichphant, B. Inceesungvorn, N. Wetchakun, J. Alloys Compd. **597**, 129 (2014)
18. W.J. Luo, Z.S. Li, T. Yu, Z.G. Zou, J. Phys. Chem. C **116**, 5076 (2012)
19. A.L. Pacquette, H. Hagiwara, T. Ishihara, A.A. Gewirth, J. Photochem. Photobiol., A **277**, 27 (2014)
20. Y. Ji, J. Cao, L. Jiang, Y. Zhang, Z. Yi, J. Alloys Compd. **590**, 9 (2014)
21. W. Wang, J. Wang, Z. Wang, X. Wei, L. Liu, Q. Ren et al., J. Chem. Soc., Dalton Trans. **43**, 6735 (2014)
22. H.Q. Jiang, H. Endo, H. Natori, M. Nagai, K. Kobayashi, Mater. Res. Bull. **44**, 700 (2009)
23. Y. Xie, G. Ali, S.H. Yoo, S.O. Cho, A.C.S. Appl, Mater. Interfaces. **2**, 2910 (2010)